

Electronic Supplementary information: Modulation of photoacoustic NIR BODIPY self-assembly in theranostic solid lipid nanoparticles via alpha-group variation: influence on spectral and nanostructural properties

Clément Linger,^{a,b} Frédéric Gobeaux,^c Mathieu Lordez,^{a,d,e} Justine Coïs,^d Rachel Méallet,^e Gilles Clavier,^d Nicolas Tsapis,^{‡*a} and Jérôme Gateau ^{‡*b}

^a Université Paris-Saclay, CNRS, Institut Galien Paris-Saclay, 91400 Orsay, France.

^b Sorbonne Université, CNRS, INSERM, Laboratoire d'Imagerie Biomédicale, 75006 Paris, France.

^c Université Paris-Saclay, CEA Saclay, CNRS, NIMBE, UMR 3685, LIONS, 91191 Gif-Sur-Yvette Cedex, France.

^d Université Paris-Saclay, ENS Paris-Saclay, CNRS, PPSM, 91190 Gif-sur-Yvette, France.

^e Université Paris-Saclay, CNRS, Institut des Sciences Moléculaires d'Orsay, 91405 Orsay, France.

Table of Content

1. MATERIAL AND METHODS.....	1
1.1. BODIPY SCAFFOLD.....	1
1.2. SYNTHESIS OF BODIPY-JULOLIDINE.....	2
1.3. SYNTHESIS OF BODIPY-JULOLIDINE-PALMITATE.	4
1.4. NANOPARTICLE FORMULATION.....	6
1.5. SYNTHESIS OF BODIPY-JULOLIDINE-PLA (BY-JULOLIDINE-PLA) AND PARTICLE FORMULATION.....	6
1.6. AUTOCORRELATION IMAGES.....	6
2. RESULTS.....	6
2.1. ABSORPTION AND FLUORESCENCE OF DYES.....	6
2.2. COLLOIDAL SUSPENSION CHARACTERISATION	7
2.3. FLUORESCENCE, ABSORPTION AND PHOTOACOUSTIC SPECTRA OF NANOPARTICLES	8
2.4. STRUCTURAL CHARACTERISATION	9
2.4.1. CRYO-EM	9
2.4.1. SAXS-WAXS FITTING PARAMETERS	12
REFERENCES.....	12

1. Material and methods

1.1. BODIPY scaffold

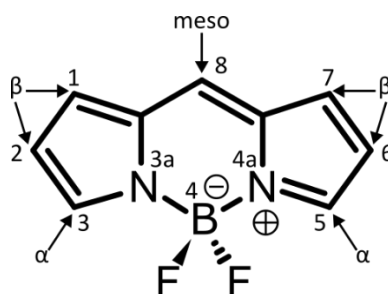


Fig. S1: BODIPY scaffold structure with official IUPAC nomenclature

1.2. Synthesis of BODIPY-julolidine.

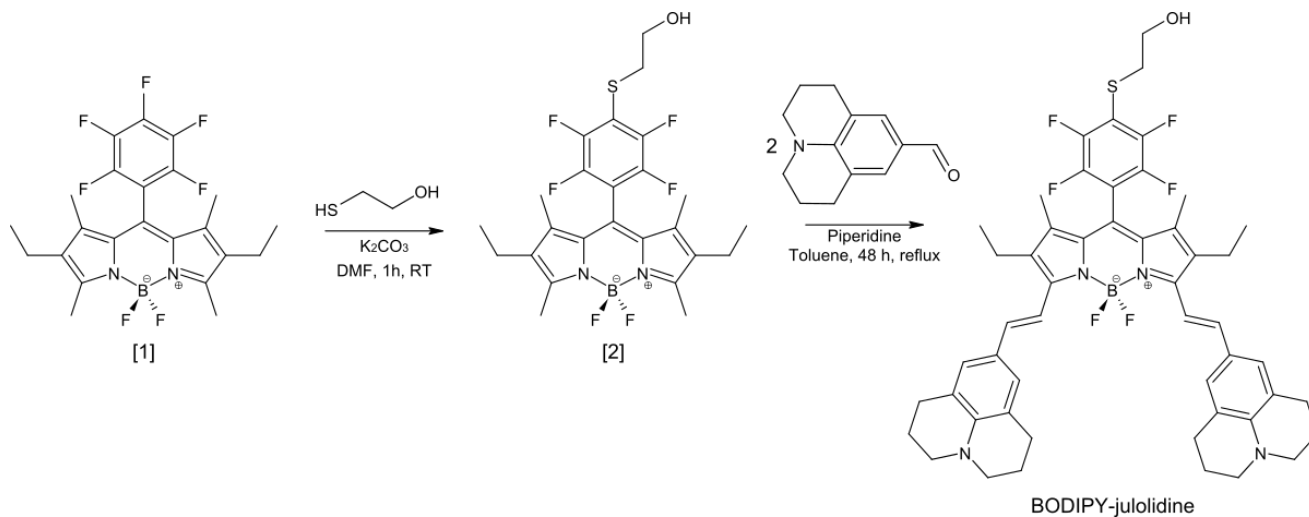


Fig. S2: Reaction scheme to form BODIPY-julolidine

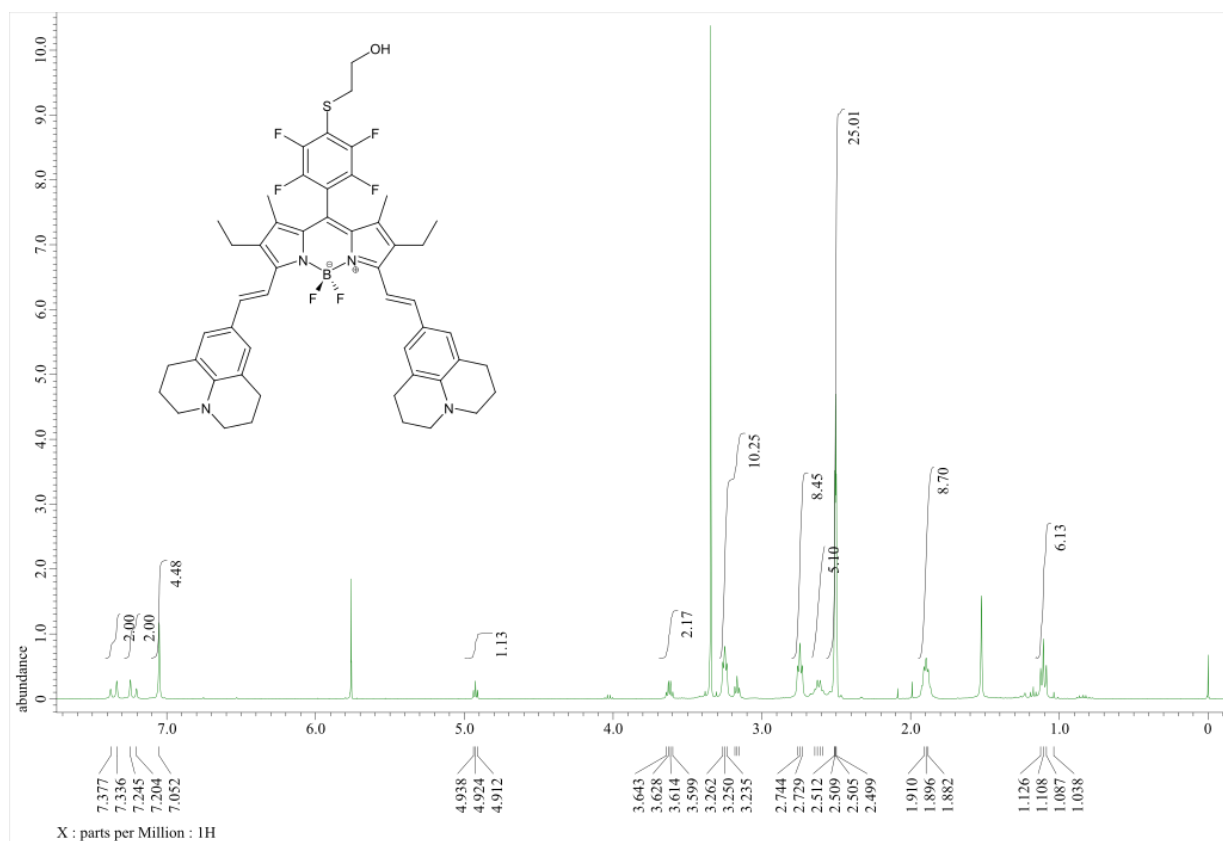


Fig. S3: ¹H NMR of BY-julolidine

1.3. Synthesis of BODIPY-julolidine-palmitate.

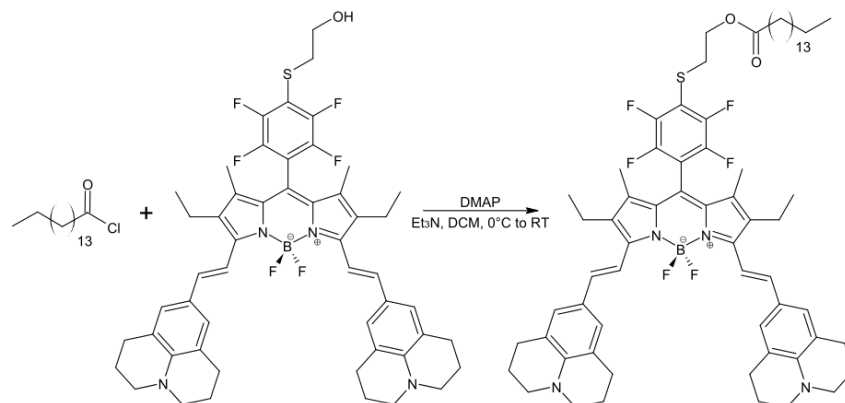


Fig. S6: Reaction scheme (esterification) to form BODIPY-julolidine-Palmitate

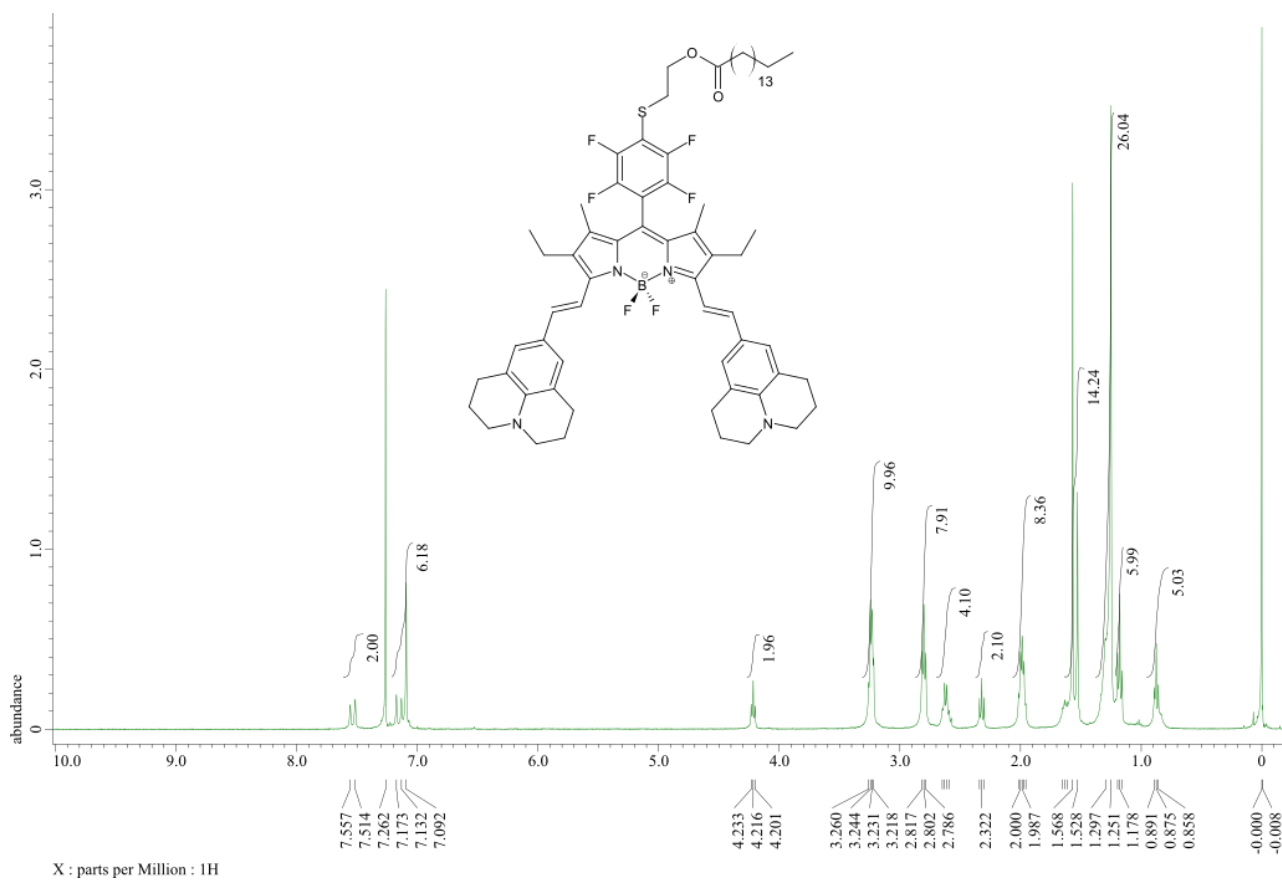


Fig. S7: ¹H NMR of BY-julolidine-Palm

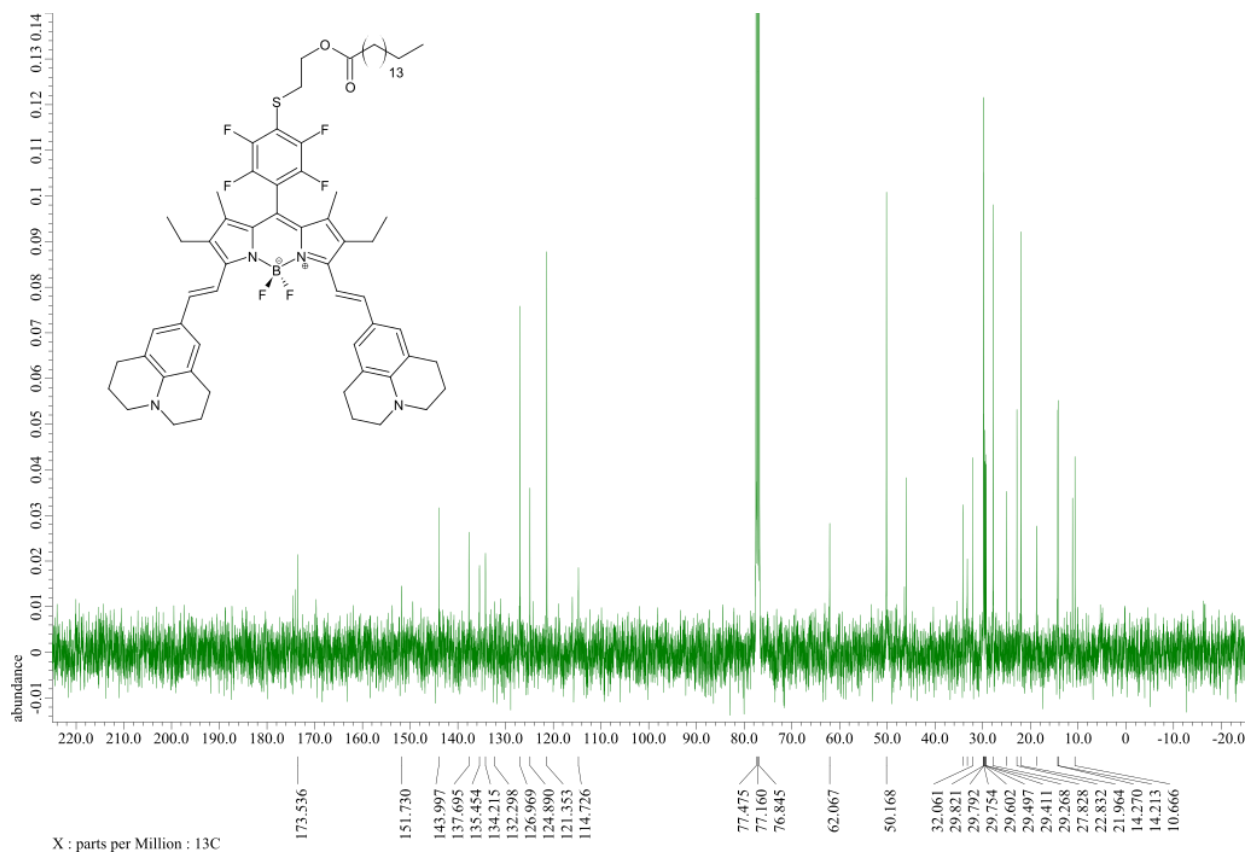


Fig. S8: ¹³C NMR of BY-julolidine-Palm

20240227_CL045_FTMS #11-41 RT: 0.02-0.08 AV: 31 NL: 1.85E8
 T: FTMS + p ESI Full ms [200.0000-2000.0000]

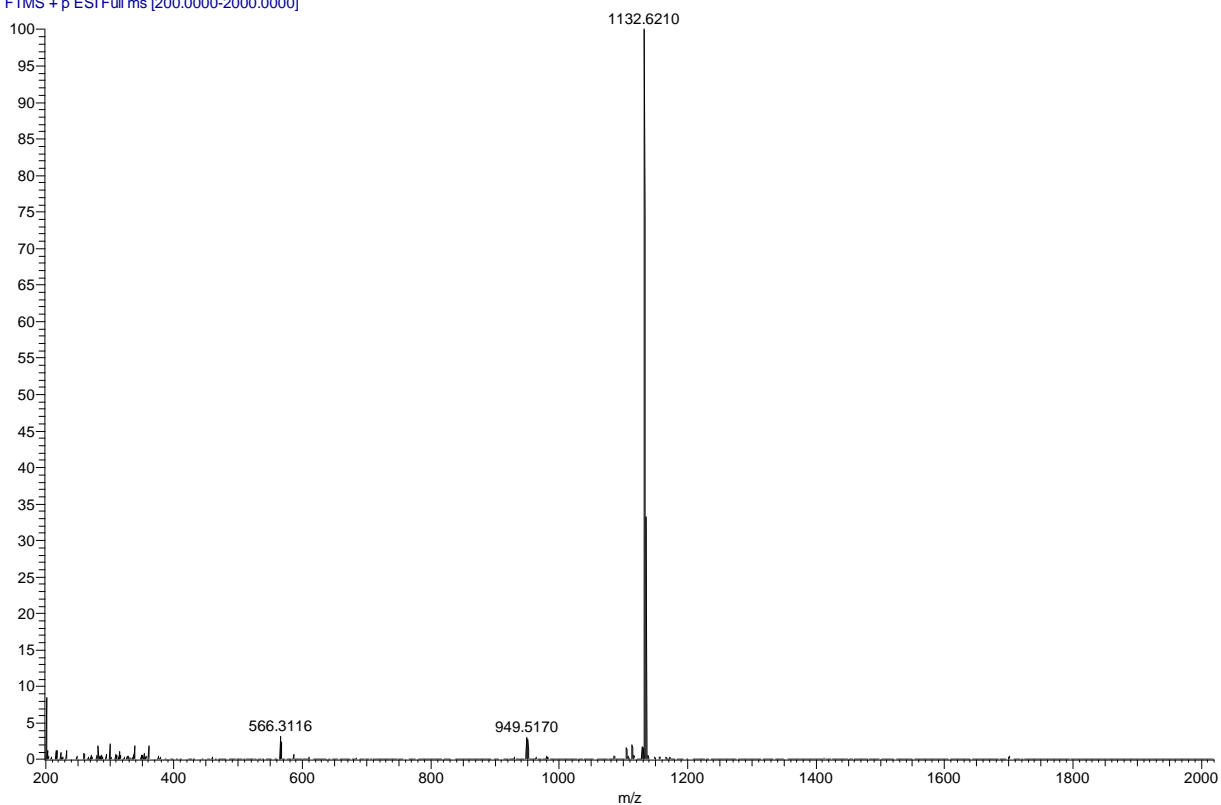


Fig. S9: HRMS (ESI) spectrum of BY-julolidine-Palm

1.4. Nanoparticle Formulation.

Table S1 – BY-Palm concentrations in SLNs and dilution factor to reach the same concentration.

	SLN-2%	SLN-25%	SLN-50%	SLN-100%
<i>BY-aniline-Palm concentration (mg.mL⁻¹)</i>	0.161	1.76	3.10	5.00
<i>BY-aniline-Palm concentration (mM)</i>	1.56.10 ⁻¹	1.71	3.01	4.86
<i>Dilution (to 1.73.10⁻² mM)</i>	9	98	175	280
<i>BY-julolidine-Palm concentration (mg.mL⁻¹)</i>	0.172	1.84	3.18	4.98
<i>BY-julolidine-Palm concentration (mM)</i>	1.52.10 ⁻¹	1.63	2.81	4.40
<i>Dilution (to 1.73.10⁻² mM)</i>	10	96	165	260

1.5. Synthesis of BODIPY-julolidine-PLA (BY-julolidine-PLA) and particle formulation

PLA-BY-aniline was prepared as described in Bodin et al ¹. Synthesis of BY-julolidine-PLA is analogous to the synthesis of BY-aniline-PLA, by ring opening polymerization of DL-lactide¹. Racemic DL-lactide (0.150 g, 1.02×10^{-3} mol, $144 \text{ g}\cdot\text{mol}^{-1}$) and initiator BY-julolidine (0.010 g, 1.12×10^{-5} mol, $895 \text{ g}\cdot\text{mol}^{-1}$) were introduced into a Schlenk under argon atmosphere. In another Schlenk, 2 drops of stannous octoate (0.0033 g, 8.1×10^{-5} mol, $405 \text{ g}\cdot\text{mol}^{-1}$) and 2.7 mL of anhydrous toluene were added. Then, 0.5 mL of the stannous octoate solution was introduced in the reagent flask. The Schlenk was heated in an oil bath at 130 °C for 2 h under argon. The reaction was then stopped with an ice bath, and toluene was evaporated during 30 min. The solid obtained was dissolved in the strict minimum of chloroform, and the solute was precipitated in 80 mL of cold diethyl ether under vigorous agitation. The supernatant was removed by centrifugation (5000 rpm, 4 °C), and the solid was dissolved in a minimum of tetrahydrofuran. The solute was once more precipitated in 80 mL of distilled water under vigorous agitation. The supernatant was removed by centrifugation (5000 rpm, 4 °C), and the solid was freeze-dried (3 or 4 days) to obtain final polymer BY-julolidine-PLA (90 mg, $17,000 \text{ g}\cdot\text{mol}^{-1}$, 56%, labelling efficiency 93%). The labelling efficiency was evaluated by NMR and by the maximum peak absorbance of PLA-BY-julolidine and compared to the BY-julolidine calibration curve in DCM.

BY-PLA-aniline-47% and BY-PLA-julolidine-47% were formulated with 11.75 mg of BY-aniline-PLA or BY-julolidine-PLA respectively and 13.25 mg of DSPE-PEG5000. This percentage was chosen because it corresponds to a BY-aniline or BY-julolidine molar concentration of 0.157 mM which is the same molar concentration as in the SLN-2%. Briefly, BY-PLA and DSPE-PEG5000 were put in 2 mL of chloroform and poured into 5 mL of a cold solution of sodium cholate (15 g/L). After 30 s of vortexing and ultrasonication in an ice bath during 1 min at an amplitude of 30 % with Sonifier SFX150 (Branson, USA), organic phase was evaporated under chemical hood for 3 h with a 300-rpm stirring. Sodium cholate was removed by ultracentrifugation for 1 h at 4 °C and 40,000 rpm (Optima LE-80K Ultracentrifuge Beckman Coulter, USA). The obtained solid was resuspended in milli-Q water to a final polymer concentration of 5 mg/mL.

BY-aniline-PLA NPs and BY-julolidine-PLA NPs exhibit similar size, polydispersity and zeta potential characteristics. For BY-aniline-PLA NPs, size (DLS): 153 ± 3 nm, Pdl (DLS): 0.15 ± 0.01 , and ζ potential: -17 ± 1 mV. For BY-julolidine-PLA NPs, size (DLS): 156 ± 4 nm, Pdl (DLS): 0.12 ± 0.01 , and ζ potential: -13 ± 2 mV.

1.6. Autocorrelation images

Autocorrelation images were obtained from the raw cryo-EM images. Image processing was performed using MATLAB (MathWorks, Inc). The ROIs were manually selected to avoid interfaces such as the surface of a particle and to favour homogeneously filled regions. For each ROI, the fluctuations with very low spatial frequencies (including the average value) were removed by subtracting a polynomial surface model of degree 1. A polynomial surface model of degree 2 was used for SLN-julolidine-100% due to stronger low spatial frequency fluctuations. The coefficients of the model were obtained with a 2-dimensional polynomial fit. The autocorrelation image was calculated and presented a sharp and intense central peak with a full-width half-maximum around 1 pixel. This central value was removed by a 2D-Gaussian fit and subsequent subtraction for the sake of readability. From the autocorrelation images, the radial average of the pixel values was numerically calculated with a 2-pixel integrative step. Finally, the local minima of the radial average were found by an analytical fit of the curve inflexions by a quadratic function.

2. Results

2.1. Absorption and fluorescence of dyes

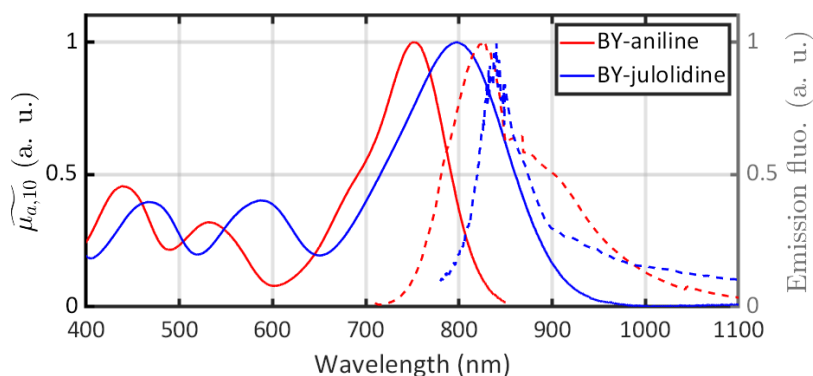


Fig. S10: Absorption (solid line) and fluorescence (dashed line) of BY-aniline (red) and BY-julolidine (blue) in DCM (arbitrary units).

2.2. Colloidal suspension characterisation

Table S2 – Nanoparticle sizes determined by dynamic light scattering (DLS), nanoparticle tracking analysis (NTA), SAXS fit and cryo-EM. Pdl and ζ potential are also given.

		Size (nm)				Pdl	ζ potential (mV)
		SAXS*	Cryo-EM	NTA	DLS	DLS	
BY-aniline	SLN-0%	50	64±38 (289)**	141±2	163±2	0.14±0.01	-43±3
	SLN-2%	54	75±33 (358)	129±1	173±1	0.14±0.01	-41±2
	SLN-25%	63	89±56 (221)	151±6	182±1	0.16±0.02	-44±1
	SLN-50%	54	NS***	203±6	229±1	0.18±0.01	-41±2
	SLN-100%	49	NS	147±3	161±1	0.28±0.01	-39±3
BY-julolidine	SLN-2%	50	86±46 (292)	128±5	178±1	0.14±0.01	-42±2
	SLN-25%	52	87±47 (354)	151±4	179±1	0.14±0.01	-41±1
	SLN-50%	52	102±53 (360)	140±3	181±2	0.12±0.02	-39±4
	SLN-100%	55	67±31 (150)	150±6	187±2	0.14±0.02	-34±2

* Median diameter

** Number of particles evaluated

*** NS: not spherical

Table S3 – Nanoparticle density number determined by nanoparticle tracking analysis (NTA) and derived average number of BY-Palm per particle ($\#$ BY-Palm/part) and absorption cross section per mole of particles ($\epsilon_{\text{particle}}$).

	BY-aniline			BY-julolidine		
	# part/L	# BY-Palm/part	$\epsilon_{\text{particle}}^*$	# part/L	# BY-Palm/part	$\epsilon_{\text{particle}}$
SLN-2%	1.8×10^{16}	5.4×10^3	2.2×10^8	1.8×10^{16}	5.1×10^3	1.9×10^8
SLN-25%	9.6×10^{15}	1.1×10^5	3.6×10^9	6.3×10^{15}	1.6×10^5	5.9×10^9
SLN-50%	1.0×10^{16}	1.8×10^5	7.7×10^9	6.3×10^{15}	2.7×10^5	9.7×10^9
SLN-100%	9.2×10^{15}	3.2×10^5	1.8×10^{10}	6.6×10^{15}	7.5×10^5	1.3×10^{10}

* $\epsilon_{\text{particle}}$: absorption cross section per mole of particles expressed in $\text{M}^{-1} \cdot \text{cm}^{-1}$ and evaluated at the maximum absorption wavelength

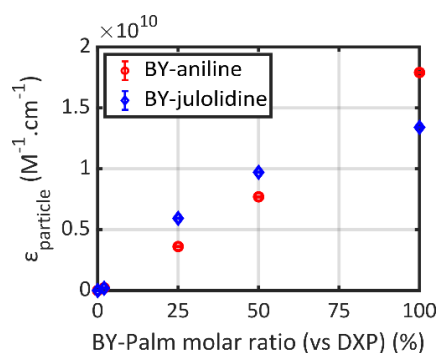


Fig. S11: Evolution of the absorption cross section per mole of particles as a function of the BY-Palm percentage. The absorbance is considered at its maximum value (and not at a fixed wavelength)

2.3. Fluorescence, absorption and photoacoustic spectra of nanoparticles

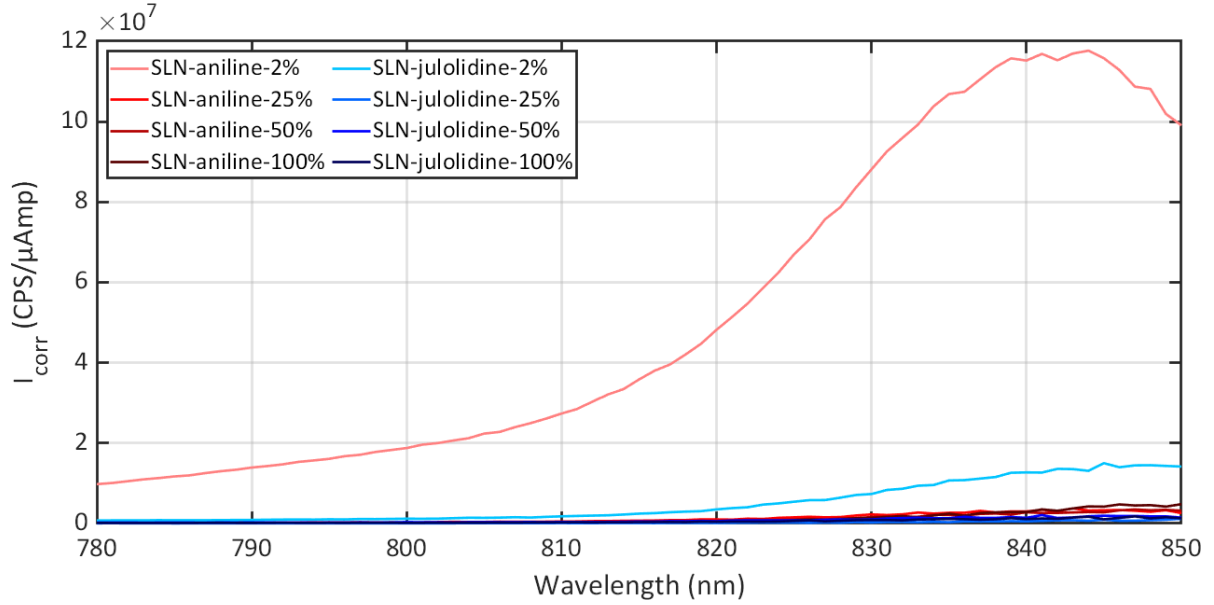


Fig. S12: Fluorescence spectrum ($\lambda_{ex} = 750$ nm, slits width 10 nm and $A < 0.1$) of each SLN. The amplitude was corrected by the absorbance at 750 nm.

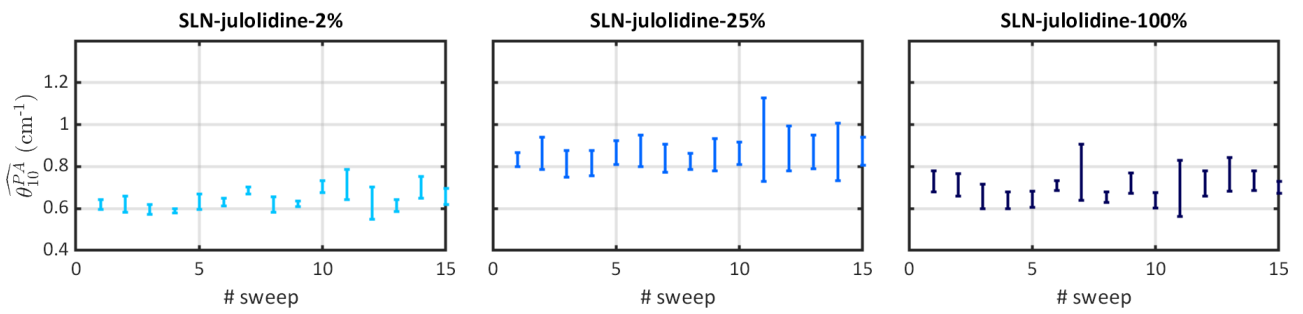


Fig. S13: Photoacoustic coefficients as a function of the sweep number. The PA coefficients are measured at the maximum absorption wavelength, namely: 800 nm for SLN-julolidine-2% (light blue), 820 nm for SLN-julolidine-25% (blue) and 830 nm for SLN-julolidine-100% (dark blue), respectively. For each sweep, the acquisition was performed simultaneously on four tubes and the displayed results corresponds to the median (with the *MAD* as error bar) over the 4 tubes.

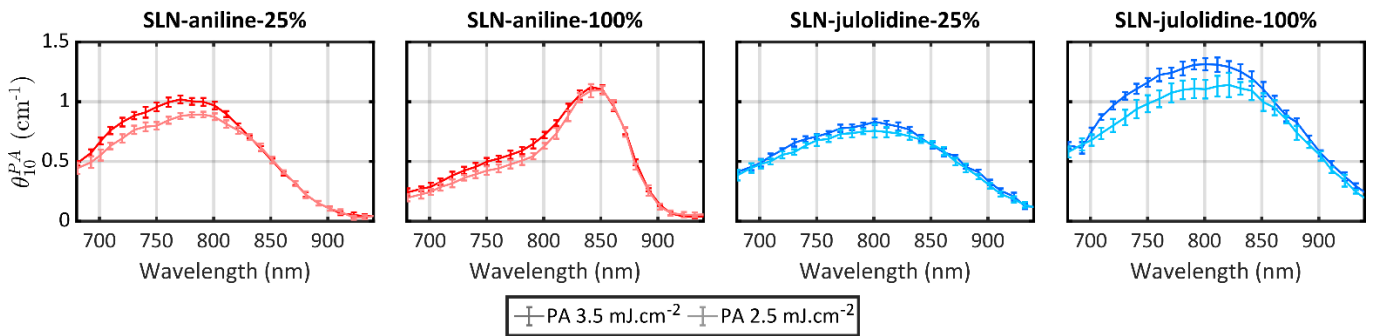


Fig. S14: Superposition of the PA for two formulations (SLN-25% and SLN-100%) in case of SLN-aniline and SLN-julolidine. Two different laser fluences were used: 3.5 $\text{mJ}\cdot\text{cm}^{-2}$ (darkest colours) and 2.5 $\text{mJ}\cdot\text{cm}^{-2}$ (lightest colours). The variation between the two fluences spectra is below 10% in mean.

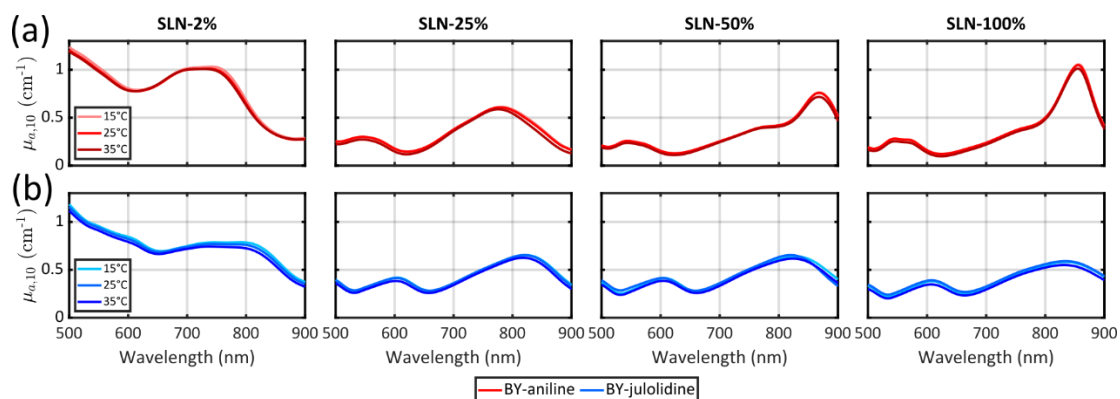


Fig. S15: Absorbance spectra measured at three temperatures (15°C, 25°C and 35°C) of (a) SLN-aniline and (b) SLN-julolidine. The scattering was not corrected.

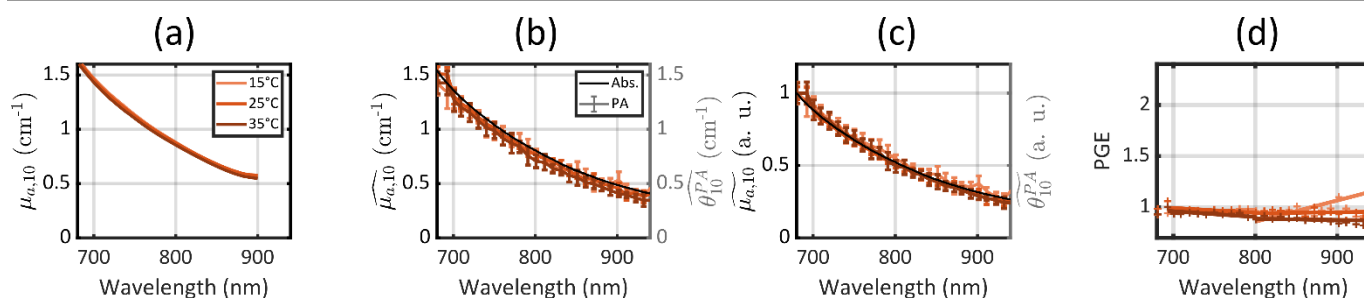


Fig. S16: (a) Absorption spectra measured at three temperatures (15°C, 25°C and 35°C) of GNPs. The scattering was not corrected. (b) Absorption spectra (black) and PA spectra at three temperatures (15°C, 25°C and 35°C) of GNPs normalized by the spectrum maximum. (c) Absorption spectra (black) and PA spectra at three temperatures (15°C, 25°C and 35°C) of GNPs normalized by the spectrum maximum. (d) PGE of GNPs at each temperature with linear regression from 690 nm to 800 nm and from 800 nm to the last measurable point. Vertical scale bar has been intentionally kept as in Fig. 4 to facilitate the comparison. The colour code is the same in (a), (b), (c) and (d).

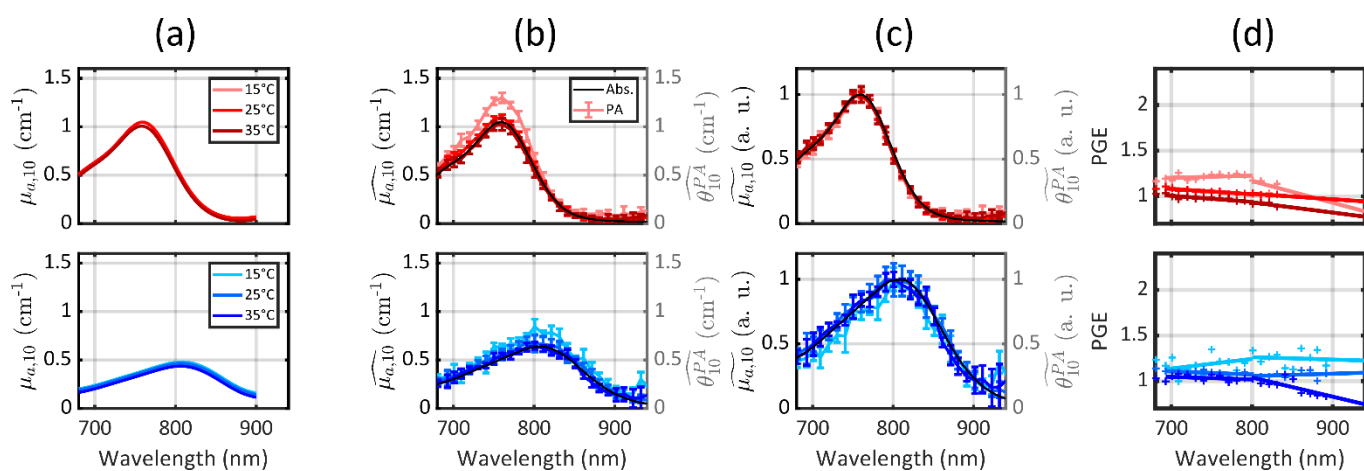


Fig. S17: (a) Absorption spectra measured at three temperatures (15°C, 25°C and 35°C) of PLA NPs (shade of red for BY-aniline and of blue for BY-julolidine). The scattering was not corrected. (b) Absorption spectra (black) and PA spectra at three temperatures (15°C, 25°C and 35°C) of PLA NPs. (c) Absorption spectra (black) and PA spectra at three temperatures (15°C, 25°C and 35°C) of PLA NPs normalized by the spectrum maximum. (d) PGE of PLA NPs at each temperature with linear regression from 690 nm to 800 nm and from 800 nm to the last measurable point. Vertical scale bar has been intentionally kept as in Fig. 4 to facilitate the comparison. The colour code is the same in (a), (b), (c) and (d).

2.4. Structural characterisation

2.4.1. Cryo-EM

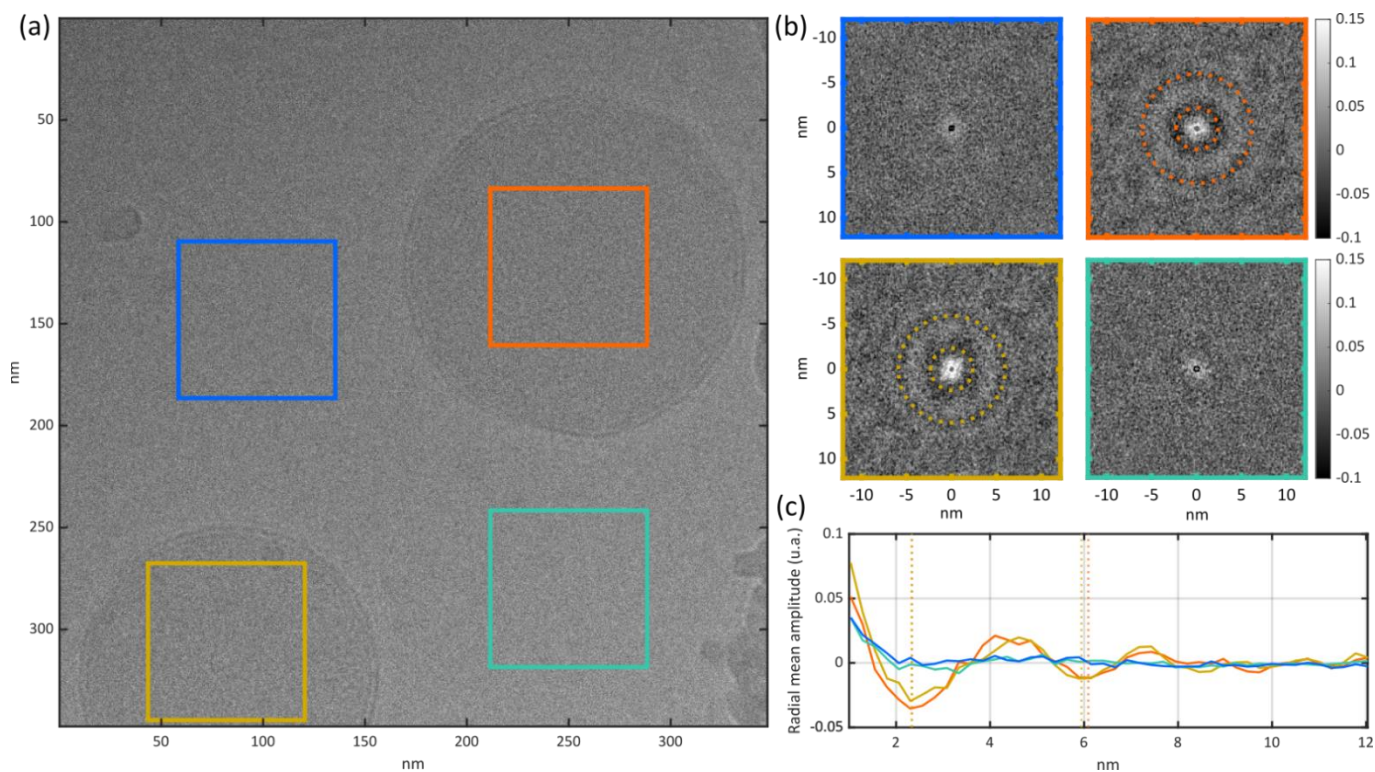


Fig. S18: Cryo-EM image analysis for SLN-0%. (a) Cryo-EM image of SLN-0% with four ROIs, each delimited by a square box. The yellow and orange boxes define ROIs inside particles and the blue and green boxes correspond to the background outside the particles. (b) 2D autocorrelation images calculated for the 4 ROIs identified in (a). The central pixel of the autocorrelation images was cropped and the grayscale range was adapted for the sake of readability of the images. For the autocorrelation images of ROIs inside the particles, dotted circles with radius corresponding to minima in the radial average of the autocorrelation are displayed and highlight the radial symmetry of the autocorrelation pattern. (c) Plot of the radial average of autocorrelation images. The vertical dotted lines indicate the radius of the minima.

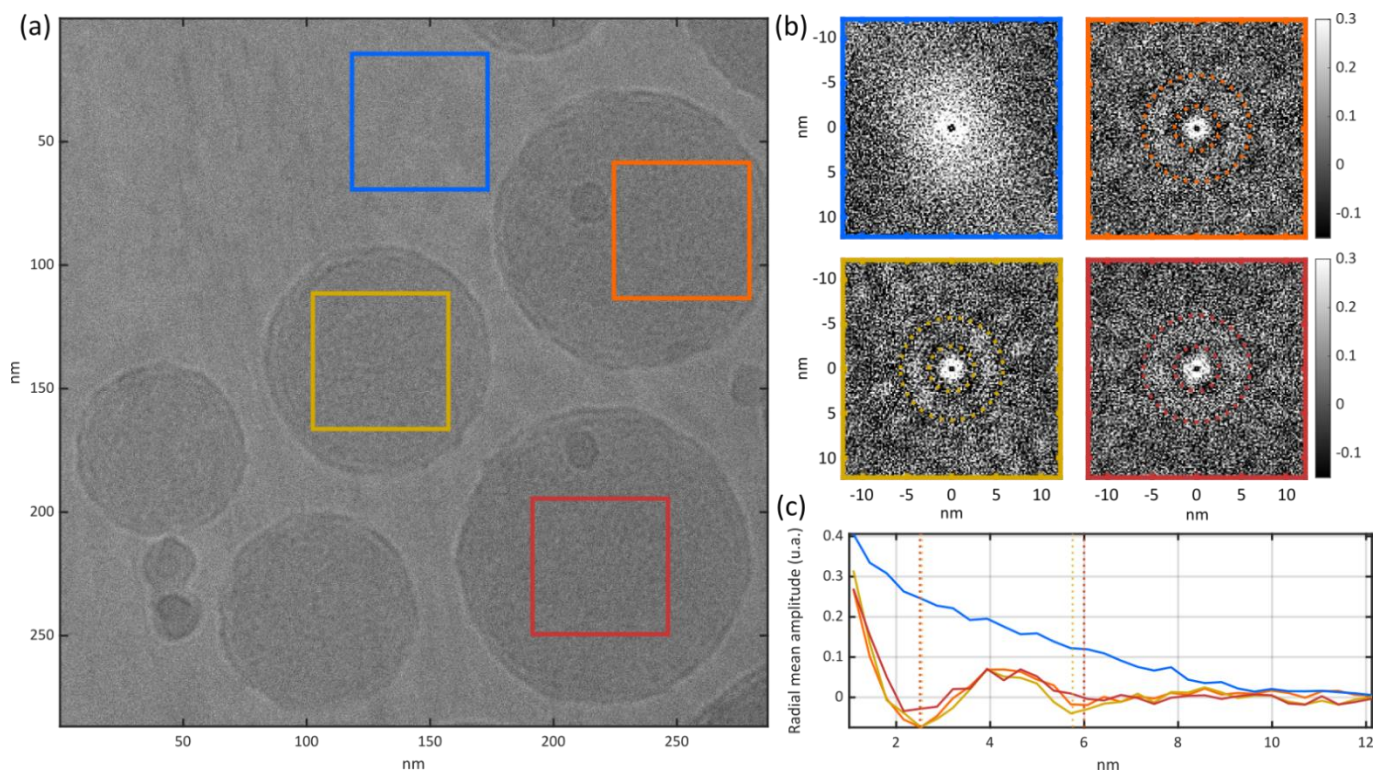


Fig. S19: Cryo-EM image analysis for SLN-aniline-25%. (a) Cryo-EM image of SLN-aniline-25% with four ROIs, each delimited by a square box. The yellow, orange and red boxes define ROIs inside particles and the blue box corresponds to the background outside the particles. (b) 2D autocorrelation images calculated for the 4 ROIs identified in (a). The central pixel of the autocorrelation images was cropped and the grayscale range was adapted for the sake of readability of the images. For the autocorrelation images of ROIs inside the particles, dotted circles with radius corresponding to minima in the radial average of the autocorrelation are displayed and highlight the radial symmetry of the autocorrelation pattern. (c) Plot of the radial average of autocorrelation images. The vertical dotted lines indicate the radius of the minima.

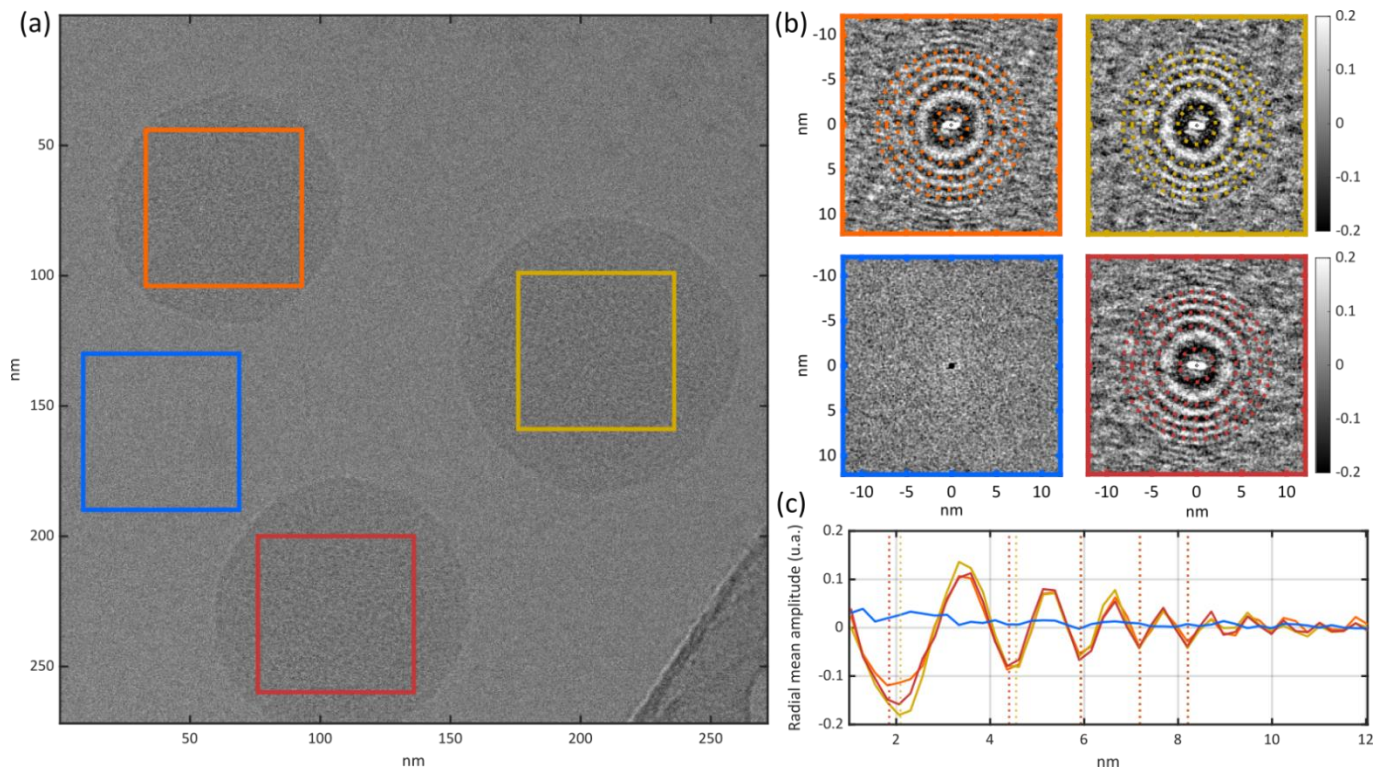


Fig. S20: Cryo-EM image analysis for SLN-julolidine-25%. (a) Cryo-EM image of SLN- julolidine-25% with four ROIs, each delimited by a square box. The yellow, orange and red boxes define ROIs inside particles and the blue box corresponds to the background outside the particles. (b) 2D autocorrelation images calculated for the 4 ROIs identified in (a). The central pixel of the autocorrelation images was cropped and the grayscale range was adapted for the sake of readability of the images. For the autocorrelation images of ROIs inside the particles, dotted circles with radius corresponding to minima in the radial average of the autocorrelation are displayed and highlight the radial symmetry of the autocorrelation pattern. (c) Plot of the radial average of autocorrelation images. The vertical dotted lines indicate the radius of the minima.

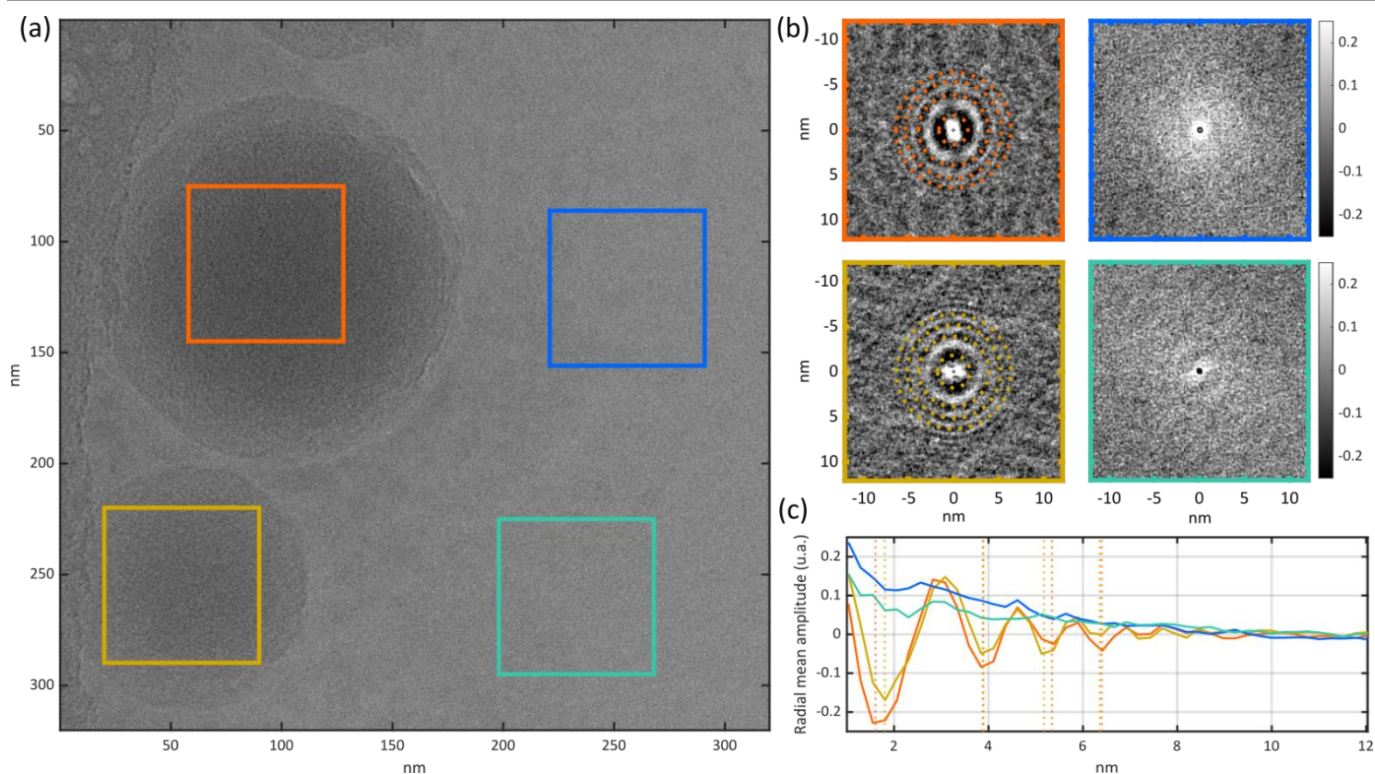


Fig. S21: Cryo-EM image analysis for SLN-julolidine-100%. (a) Cryo-EM image of SLN- julolidine-100% with four ROIs, each delimited by a square box. The yellow and orange boxes define ROIs inside particles and the blue and green boxes correspond to the background outside the particles. (b) 2D autocorrelation images calculated for the 4 ROIs identified in (a). The central pixel of the autocorrelation images was cropped and the grayscale range was adapted for the sake of readability of the images. For the autocorrelation images of ROIs inside the particles, dotted circles with radius corresponding to minima in the radial average of the autocorrelation are displayed and highlight the radial symmetry of the autocorrelation pattern. (c) Plot of the radial average of autocorrelation images. The vertical dotted lines indicate the radius of the minima.

2.4.1. SAXS-WAXS fitting parameters

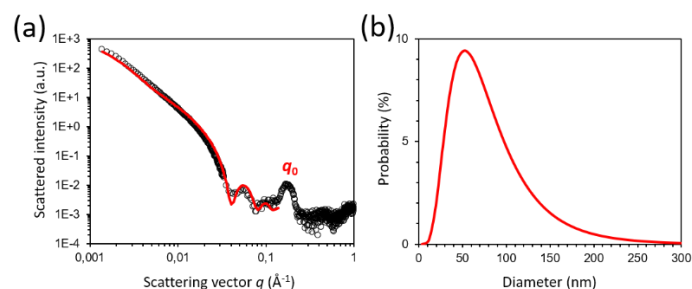


Fig. S22: (a) SAXS-WAXS pattern of SLN-0% (open circles) and its fit with a model of polydisperse vesicles (red trace). (b) Lognormal distribution (Pdl = 0.55) of the SLN-0% diameter obtained from the fit.

Table S4 – SAXS and WAXS fitting parameters. The diameter and the polydispersity were obtained by fitting the SAXS pattern with an assembly of polydisperse spheres. The interlayer spacing $d(q_0)$ and the correlation length were obtained by fitting the first peak of the WAXS diagram with a Gaussian peak.

		Diameter (nm)		$d(q_0)$ (nm)	ξ (nm)
		Fresh	3-month aging		
BY-aniline	SLN-0%	50	71	3.72	10.43
	SLN-2%	54	74	3.65	9.86
	SLN-25%	63	58	3.95	7.29
	SLN-50%	NA*	NA	3.83	8.23
	SLN-100%	NA	NA	3.53	31.18
BY-julolidine	SLN-2%	50	71	3.77	9.06
	SLN-25%	52	56	3.72	7.95
	SLN-50%	52	60	4.11	4.78
	SLN-100%	55	62	NA	NA

* NA: not applicable

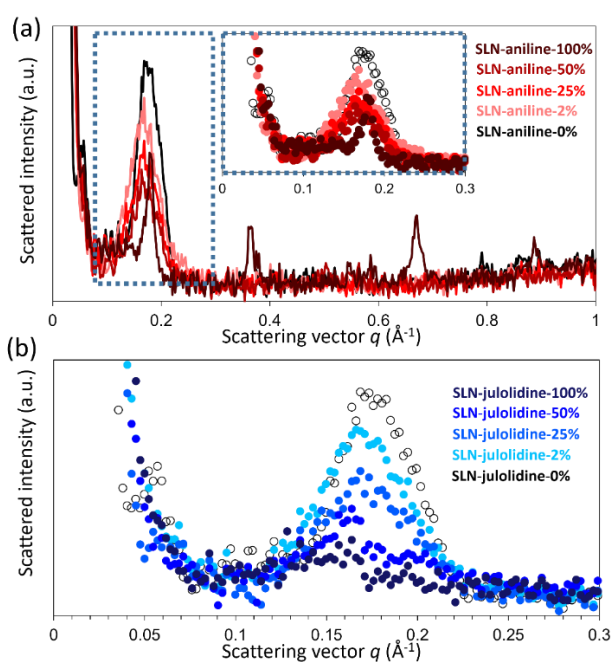


Fig. S23: (a) WAXS characterization of SLN-aniline for SLN-2%, SLN-25%, SLN-50% and SLN-100%. The inset is a blow-up of the first order diffraction peak. (b) WAXS characterization of SLN-julolidine for SLN-2%, SLN-25%, SLN-50% and SLN-100% (blow-up of the first order diffraction peak).

References

1 J.-B. Bodin, J. Gateau, J. Cois, T. Lucas, F. Lefebvre, L. Moine, M. Noiray, C. Cailleau, S. Denis, G. Clavier, N. Tsapis and R. Méallet-Renault, *ACS Appl. Mater. Interfaces*, 2022, 40501–40512.